IEEE Access
Multidisciplinary | Rapid Review | Open Access Journal

Received 29 February 2024, accepted 28 May 2024, date of publication 31 May 2024, date of current version 7 June 2024.

Digital Object Identifier 10.1109/ACCESS.2024.3408081

RESEARCH ARTICLE

Nonlinear Microwave Susceptibility Measurements Using Intermodulation Products on a Microfluidic Platform

CÉSAR PALACIOS-ARIAS[1], (Student Member, IEEE), MARC JOFRE[2], MARÍA-JOSÉ LÓPEZ[1], (Student Member, IEEE), YOUNESS AKAZZIM[1], (Student Member, IEEE), LLUIS JOFRE[3], JORDI ROMEU[1], (Fellow, IEEE), AND LUIS JOFRE-ROCA[1], (Life Fellow, IEEE)

[1]Department of Signal Theory and Communications, Universitat Politècnica de Catalunya—BarcelonaTech (UPC), 08034 Barcelona, Spain
[2]Department Network Engineering, Universitat Politècnica de Catalunya—BarcelonaTech (UPC), 08860 Barcelona, Spain
[3]Department of Fluid Mechanics, Universitat Politècnica de Catalunya—BarcelonaTech (UPC), 08019 Barcelona, Spain

Corresponding author: César Palacios-Arias (cesar.augusto.palacios@upc.edu)

This work was supported in part by the Agencia Estatal de Investigación, Spain, under Grant PID2019-107885GB-C31, Grant PID 2022-136869NB-C31, and Grant PDC2022-133091-I00; in part by the Generalitat de Catalunya, Spain, under Grant PDR-2014-2022/56-30157-2021-2A; in part by the ''Formación de Personal Investigador'' Scholarship under Grant PID2019-107885GB-C31 and Grant PRE2020-093895; and in part by the Beatriz Galindo Program of the Ministerio de Ciencia, Innovación y Universidades, Spain, under Grant BGP18/00026.

ABSTRACT Measuring the nonlinear responses of living cells has enabled an understanding of their behavior and functionality. Currently, this response has been studied at radio and optical frequencies, leaving an unexplored gap in the field of microwaves. This paper presents a system that combines microwave technology with a microfluidic platform to measure the nonlinear susceptibility of living organisms to electromagnetic fields. The applied technique involves feeding the system with two tones (2.1 GHz and 4 GHz) to generate third-order intermodulation products (PIMP) at 5.9 GHz. Nonlinear susceptibility was measured from the power levels of PIMP using a spectrum analyzer. Broadband electrodes based on the slot bowtie geometry were manufactured to operate at 5 GHz with a bandwidth of 4 GHz. Additionally, an engineering process is presented to optimize the power of the internal mixer of the spectrum analyzer to obtain the maximum dynamic range and improve the sensitivity of the system. Nonlinear susceptibility to microwaves was analyzed in four samples: pure ethanol, a mixture of ethanol and dimethyl sulfoxide (DMSO), live Escherichia coli (E. coli), and heat-killed E. coli. The results show that ethanol has zero nonlinear susceptibility, whereas when it is mixed with DMSO, a nonlinear response appears at a value of 4 dB with respect to the nonlinear susceptibility of the system in the absence of a sample. Finally, the nonlinear susceptibility of live E. coli to microwaves was detected, with a difference of 8 dB over the reference value and 6 dB with respect to the heat-killed E. coli sample.

INDEX TERMS E. coli, intermodulation products, microfluidic, microwave, nonlinear susceptibility, non-invasive, power, spectrum analyzer.

I. INTRODUCTION

In recent years, there has been growing interest in rapid, non-invasive, and highly sensitive mechanisms for the determination of cellular properties [1]. In this sense, the integration of microwave and microfluidic technologies has shown great potential for real-time cellular analysis by expanding the knowledge about their operation and behavior [2]. The implications of these findings cover a wide range of fields such as medicine, industry, pharmacy, and research.

The associate editor coordinating the review of this manuscript and approving it for publication was Lei Zhao.

Recent studies have highlighted the potential of microfluidic-based microwave sensors. For instance, a review of microfluidics-based microwave sensors emphasized their potential for highly sensitive, rapid, and non-invasive measurements [3]. Furthermore, the applications and increasing trend of utilizing microfluidic-microwave devices have been presented by [4] and [5]. Additionally, research on wireless microwave sensing of bacterial membrane potential in microfluidic-actuated platforms has also been presented, providing a rationale for nonlinear membrane responses [6], [7].

The nonlinear characteristics of living cells have also been studied. From a mechanical point of view, the deformation and transmission of force due to external stimuli have been studied in microorganisms [8] as well as their viscoelastic properties [9].

Regarding the interplay with electromagnetic fields, different experimental methods and theoretical models have been developed for radio frequencies (RF). For example, Chen et al. [10] characterized the nonlinear dipolarized responses of living cells based on the modulation of the applied frequency within a microfluidic device. Kuznetsov and Kuznetsova [11] developed a nonequilibrium thermodynamic theory to describe nonlinear RF interactions in living cells and their effects on molecular properties. Bartoli et al. [12] measured vibrational modes in living human cells using advanced microcantilever technology. Antonacci et al. [13] performed noncontact mechanical and chemical analyses of single living cells using spectroscopic techniques. Moreover, at optical frequencies, the nonlinear susceptibility tensor has been utilized to generate a second-order signal, which aids in sensing the action potential variation in cells [14], [15]. This principle has also been applied in Nonlinear Optical Microscopy (NLOM), a technique that generates images through nonlinear interactions between light and matter [16], [17], [18]. NLOM has proven instrumental in studying various cellular functions, including protein interactions, tissue engineering, and bacterial biofilm formation [19], [20].

Accordingly, the nonlinear electromagnetic response of living cells to radio frequency (RF) and optical electromagnetic frequencies has been thoroughly explored in existing literature. In contrast, this study addresses the existing gap by investigating this nonlinear microwave susceptibility of living cells.

Passive intermodulation products (PIMP) are the result of the nonlinear behavior of a system subjected to multiple impinging frequencies. These products consist of second- and higher-order sums and frequency differences from the original signals [21], [22]. In the context of electromagnetic systems, PIMP can be used to measure and characterize the nonlinearity of the system; therefore, it can provide valuable information on the nonlinear susceptibility characteristics of cells [23], [24], [25].

Thus, this study aims to: (i) propose a microwave-microfluidic system for real-time, non-invasive assessment of the electromagnetic nonlinear response of cells using microwave PIMP techniques, (ii) explore the system's capability to capture nonlinear responses in various samples and their dynamics under external stimuli, (iii) showcase the system's applicability in studying the nonlinear behavior of cells, and (iv) validate its potential for advancing the understanding of cellular dynamics by analyzing microwave-induced nonlinear responses.

The remainder of this paper is organized as follows: Section II provides a description of the theoretical modeling of the system. Section III describes the methodology used in the proposed system, including the microwave PIMP-based approach and microfluidic platform. Section IV presents the experimental setup used to validate the proposed system, including a description of the experimental setup, materials and equipment used. Section V presents experimental results. Section VI discusses the interpretation of the results, a comparison with existing methods, and the limitations. Finally, Section VII concludes the paper by summarizing the contributions of the proposed system and outlining the future work.

II. THEORETICAL BACKGROUND

In this section, three fundamental concepts are explored: (i) the nonlinear response of cells generated by the transmembrane voltage, (ii) the role of PIMP in nonlinear microwave susceptibility measurements, and (iii) the instrument measurement optimization for the application of the PIMP technique in cells.

A. THE TRANSMEMBRANE VOLTAGE

The electromagnetic behavior of cellular and intracellular membranes is distinctly nonlinear, and is attributed to phenomena such as the potential barrier resulting from the variance between the inner and outer electrolytes, nonlinear membrane capacitance, voltage-gated lipid membrane permeability, conductance rectification, and the impact of nonthermal electromagnetic interactions on the cellular sodium ion channel [26], [27], [28].

The transmembrane voltage, or transmembrane potential difference V_m, is the difference in electric potential between the internal and external parts of a biological cell. This potential arises from the interaction between ion channels and ion pumps embedded in the cell membrane. The membrane potential is typically of the order of $V_0 = 100\,\text{mV}$ in the absence of an applied external electromagnetic field. However, when a cell is exposed to an external electric field, it can induce transmembrane voltage excess δ_{V_m}, resulting in $V_m = V_0 + \delta_{V_m}$. During electric field stimulation, the electric current density J_m through the cell membrane was obtained by summing the capacitive current $C_m V_m$ and conduction current $\sigma_m(V_m + V_0)/d_m$, where C_m is the membrane capacitance, σ_m is the membrane conductivity, and d_m is the membrane thickness. The membrane capacitance can be calculated as $C_m = C_0 + \beta(\Delta V_m)^2$, where β is the dielectric dispersion (considering real and imaginary values)

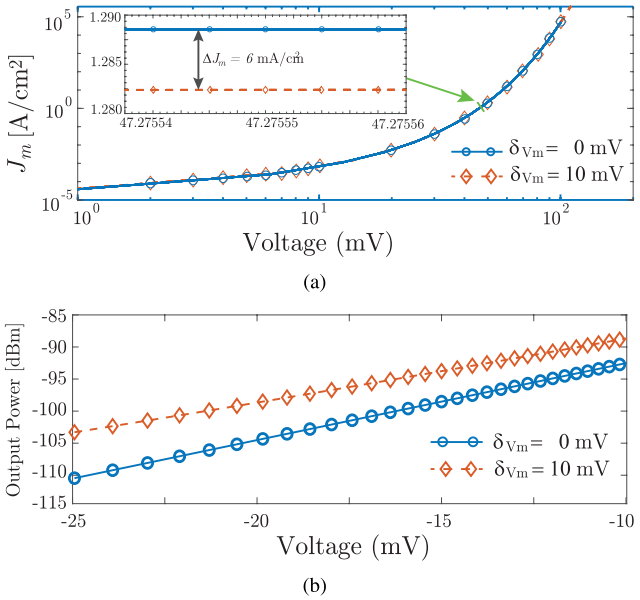

FIGURE 1. (a) Current-Voltage response for the diode-based model of a live and dead cell. The inset plot shows the current density. (b) Theoretical estimation for nonlinear susceptibility of E. coli.

of the biological cell [29]. Furthermore, for frequencies below 100 kHz, β becomes negligible and the current-voltage step-response is known to be approximated by a nonlinear diode-like relationship of the form

$$J_m = J_0[\exp(V_m/V_T) - 1], \tag{1}$$

where J_0 and V_T have typical values [25], [30] of 10^{-5}A/cm^2 and (approximately) 5mV, respectively. Moreover, considering the V_m dependence on C_m, the Maxwell stress tensor from the capacitor charges alters its geometry, for example, by reducing d_m and increasing C_m [31]. Thus, C_m exhibits a nonlinear response to V_m [32].

Figure 1 presents a current-voltage graph and the frequency harmonics generated by a bacterium when subjected to an external field. δ_{V_m} was set to approximately 10 mV for living cell and 0 mV for dead cells. Figure 1(a) illustrates the model responses under both the conditions. Moreover, to highlight the difference in current density, Fig. 1(a) provides an amplified view, revealing an estimated current-density difference of 6 mA/cm^2.

B. THIRD-ORDER PIMP GENERATION

In the linear operation range of a receiver, that is, a spectrum analyzer, the output signals increase proportionally with the input level until the system goes into compression and the output stops increasing. This is where PIMP arises as the sum and difference of the input signals according to $Mf_1 \pm Nf_2$, where M and N can be any integer number and the sum $(M + N)$ indicates the order of the products. For instance, the third order is found at $2f_1 \pm f_2$, $2f_2 \pm f_1$, $3f_1$ and $3f_2$.

To theoretically estimate the nonlinear microwave susceptibility of the cell, the generated current can be modeled in a manner similar to Eq. 1 where $I_m = I_0[\exp(V_m/V_T) - 1]$. If the system is directly excited with two sinusoidal signals of the same amplitude V_0 and frequency components of $\omega_1 = 2\pi f_1$ and $\omega_2 = 2\pi f_2$, then the current output can be obtained using the Taylor expansion as follows:

$$\begin{aligned} I_m(t) = {} & a_2 V_m^2 + (a_1 V_m + \frac{9}{4} a_3 V_m^3)\cos(\omega_{1,2} t) \\ & + \frac{1}{2} a_2 V_m^2 \cos(2\omega_{1,2} t) + \frac{1}{4} a_3 V_m^3 \cos(3\omega_{1,2} t) \\ & + a_2 V_m^2 \cos(\omega_1 \pm \omega_2) + \frac{3}{4} a_3 V_m^3 \cos(2\omega_{1,2} \pm \omega_{1,2}), \end{aligned} \tag{2}$$

The term $I_{\text{PIM3}} = \frac{3}{4} a_3 V_m^3 \cos(2\omega_{1,2} \pm \omega_{1,2})$ is the third-order intermodulation product that creates a voltage drop in the internal resistor of the function generator R_s, which is typically 50 Ω. The power P_{PIMP} can be computed using the following equation:

$$P_{\text{PIMP}} = R_g \frac{I_{\text{PIMP}}^2}{2} \tag{3}$$

Then, by varying δ_{V_m} the nonlinear microwave susceptibility can be computed in terms of the third-order intermodulation products. Figure 1(b) plots the individual input powers of the two tones versus the PIMP power with a value of $a_3 = 10^{-8}$ for $\delta_{V_m} = 0$ and $\delta_{V_m} = 10$ mV.

The power of the third-order PIMP increases three times faster than that of the input signals. Thus, a 1 dB input signal increase results in a 3 dB PIMP level rise, reducing the power difference ΔP between the input signal and the third-order PIMP by 2 dB.

III. ENHANCING INSTRUMENT PERFORMANCE FOR PIMP MEASUREMENTS

The power difference ΔP between the input power level and the PIMP harmonics is defined as the Intermodulation Free Dynamic Range (IMFDR). In this context, PIMP serves as a technique to boost the sensitivity of the spectrum analyzer when dealing with nonlinear samples, thereby optimizing the dynamic range. In this study, source 1 was set to $f_1 = 2.1$ GHz and source 2 to $f_2 = 4$ GHz, with frequency separation Δ_f and power $P_{f_1} = P_{f_2} = -19.3$ dBm. The third-order PIMP component is located at $2f_2 - f_1 = 5.9$ GHz with a measured power of $P_{f_{\text{IM}}} = -98.4$ dBm and initial IMFDR=79.1 dB. Figure 2 shows the power of the two input signals and the selected PIMP frequency.

The intermodulation free dynamic range (IMFDR) refers to the range within which a system can operate without third-order intermodulation products exceeding the noise floor of the system. A dynamic range chart visually determines the maximum dynamic range and optimal mixer power considering the third-order intercept point (TOI), Phase Noise (PN), and average noise level (DANL) related to the resolution bandwidth (RBW). Geometric analysis of the chart's curves, shown in Fig. 3, yields equations for the

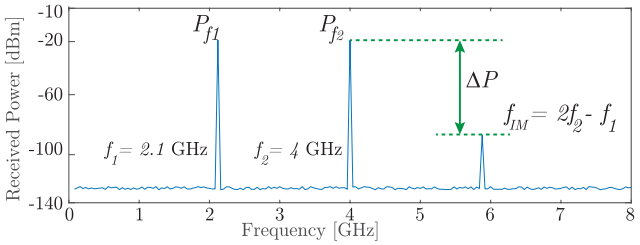

FIGURE 2. Third-order PIMP generated at $2f_2 - f_1 = 5.9$ GHz. The IMFDR corresponds to the power variation between input signal and PIMP level.

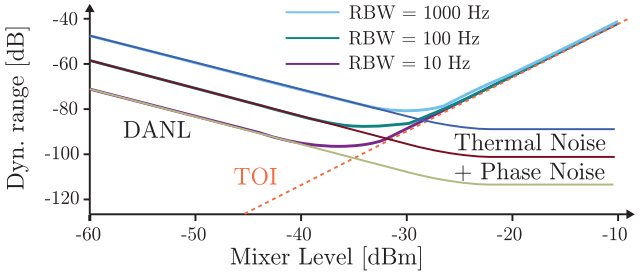

FIGURE 3. (a) Dynamic range chart of the spectrum analyzer for IMFDR as a function of input mixer level and selected resolution bandwidth.

TABLE 1. Technical specifications of the Spectrum Analyzer FSW43 (Rohde & Schwarz, Germany).

Frequency coverage	3Hz - 43 GHz
DANL	-156 dBm (at 50Hz RBW)
RBW	1Hz - 10MHz
Attenuator	0-70 dB

maximum dynamic range and optimal mixer level as

$$\mathrm{DR}_{max} = \frac{2}{3}(\mathrm{TOI} - \mathrm{DANL}) \tag{4}$$

and

$$\mathrm{MP}_{opt} = \frac{1}{3}(2\mathrm{TOI} + \mathrm{DANL}). \tag{5}$$

Using the technical data reported in Table 1, the initial and maximum dynamic range and optimum mixer power are 117.4 dB and −38.5 dBm, respectively.

A. TOI VERSUS MIXER LEVEL

The TOI is the hypothetical point at which the linear response and third-order intermodulation lines intersect after the receiver enters compression. Although the TOI cannot be measured directly, it can be calculated from the known line slopes and the measured space between the intermodulation signals and input signals P_{f_n}, according to

$$\mathrm{TOI} = \frac{\Delta P}{2} + P_{f_n}, \tag{6}$$

which results in a value of 20.17 dBm.

The dynamic range chart (Fig. 3) shows that the slope of the TOI line is +2, indicating a 2 dB decrease in the dynamic range for each 1 dB increase in fundamental tone power; the y-axis intersection at 0 dBc is equal to the TOI value.

B. DANL VERSUS MIXER LEVEL

The measurement process employed narrow-span spectral analysis controlled by the RBW, enhancing the noise signal ratio and dynamic range without affecting the scan time. Minimizing the video bandwidth (VBW) filter mitigates PIMP variation near the noise floor. In this regard, as shown in Fig. 3, the DANL relative to the mixer-level power has a −1 slope, indicating a 1-dB S/N decrease for each 1-dB power reduction in the input mixer. At 0 dBc on the y-axis, the x-axis mixer level is equal to the 1-Hz RBW DANL with 0-dB input attenuation. As a result, the noise floor increases by 10 dB for every tenfold RBW increase, and by 10 and 30 dB for 10 Hz and 1 kHz settings, respectively, compared to the 1 Hz RBW. The spectrum analyzer's DANL for this study was −156 dBm at a 5 Hz RBW with 0 dB input attenuation.

C. PHASE NOISE EFFECT ON DYNAMIC RANGE

Phase noise originating from the electrodes or the spectrum analyzer can obscure the PIMP if it coincides with the phase noise skirt. Similar to broadband noise, the phase noise floor varies with the RBW. Thus, signals displayed on a log-power scale (Video) require a −2.26 dBc phase-noise offset owing to the averaging scale. For a 1 GHz signal, the phase noise of the spectrum analyzer was approximately −104 dBc at a normalized 50 Hz RBW (Fig. 3).

D. VALID MEASUREMENT RANGE

As shown in Fig. 4, a custom dynamic range chart adjusts the mixer power and dynamic range for third-order PIMP measurements in living cells. In real scenarios, the cell PIMP frequencies align with the system PIMP frequencies, adding voltages with unknown phases. In particular, in-phase signals can display amplitudes 6 dB higher than those of the individual contributors. Equal-amplitude signals that are 180° out of phase can cancel out, displaying no distortion product. The linear uncertainty was calculated as follows:

$$u = 20\log_{10}(1 \pm 10^{P_{\mathrm{eff}}/20}). \tag{7}$$

Then, assuming an error uncertainty of less than 1 dB, and solving Eq. 7 for P_{eff}, it is possible to determine the shift adjustment of the TOI as

$$P_{eff} = 20\log_{10}(10^{u/20} - 1) = -18.3\,\mathrm{dB} \tag{8}$$

and the effective $\mathrm{TOI}_{\mathrm{eff}}$ of the spectrum analyzer is given by

$$\mathrm{TOI}_{\mathrm{eff}} = \mathrm{TOI} + (P_{\mathrm{eff}}/2) = 11.03\,\mathrm{dBm}. \tag{9}$$

The TOI line was shifted according to Eq. 8. A new optimum mixer level and intermediate maximum dynamic range can be computed using the $\mathrm{TOI}_{\mathrm{eff}}$ value according to Eq. 4 and Eq. 5, that gives as a result 111.35 dB and −44.64 dBm, respectively. The dynamic range difference was 6.09 dB. Thus, to reduce the measurement error, the optimum mixer level was shifted down in power by 6.09 dB, and the final valid measurement range corresponded to the colored region in Fig. 4.

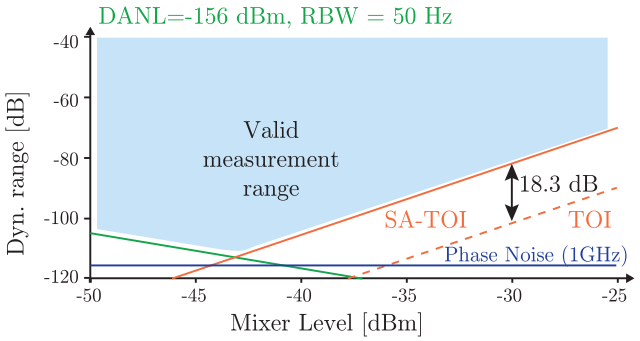

FIGURE 4. Intermodulation-free dynamic range as a function of input mixer level and selected resolution bandwidth for living cell nonlinear measurements.

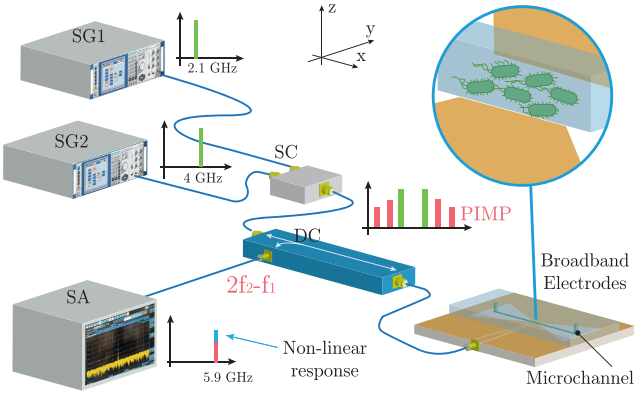

FIGURE 5. Set-up of the nonlinearities measurement system based on passive intermodulation product.

IV. DESCRIPTION OF THE SYSTEM

The system of this work is presented in three main blocks: (i) measurement of microwave intermodulation products, (ii) microfluidic control of the sample flow, and (iii) sample preparation. The first block is the proposed configuration, which is tailored for measuring passive intermodulation products at microwaves. The second block element comprises a detection platform combining microwave and microfluidic technologies based on previous research [33]. Finally, the third block details the sample preparation, aligning with the focus of this study to measure the nonlinear microwave susceptibility of living organisms.

The system is shown in Fig. 5 comprising two microwave signal generators (SG1 and SG2) (SMB100A, Rohde & Schwarz, Germany), a signal combiner (SC) (Mini-circuits, USA), a 30 dB directional coupler operating from 0.5 to 26.5 GHz (DC) (ZCDC30-5R263-S+, Mini-Circuits, USA), and a 10 MHz to 43.5 GHz spectrum analyzer (SA) (FSW43, Rohde & Schwarz, Germany). The directional coupler received a combined signal from the signal generator. This is then transmitted to the electrodes via the output port. The reflected signal was captured at the coupled port of the directional coupler and measured using the SA. To obtain optimal results, the frequency references of all sources and the analyzer were synchronized to a 10 MHz signal.

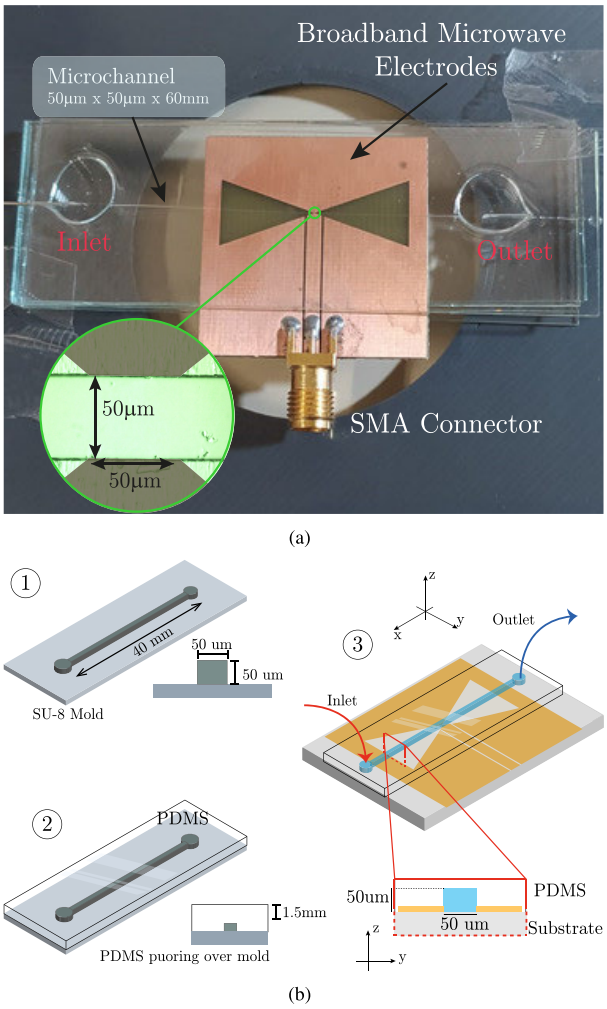

FIGURE 6. (a) Manufactured Broadband microwave electrodes and microfluidic channel. (b) Microchannel manufacturing process using soft lithography.

The electrodes were based on a slot bowtie geometry, as shown in Fig. 6 and manufactured using the RT/Duroid 4003 substrate with a relative permittivity of $\varepsilon_r = 3.55$, loss tangent of 0.9×10^{-3}, and thickness of 0.8 mm. The measured resonance frequencies of these electrodes were 5 GHz, with a bandwidth of 4 GHz. This electrode geometry was selected for its sensitivity and bandwidth characteristics, which enabled the PIMP measurements.

This study addresses the micro-scale sensing regime by incorporating a microfluidic channel of 50 µm × 50 µm in cross-section. By considering the estimated number of bacteria within each sample, determined via observation with an inverted microscope, and optimizing the flow rate to achieve a balance of hydrodynamic forces, the bacteria were constrained to focus at the centerline of the microchannel. Consequently, the particles pass through the center of the sensing volume. Accordingly, because the sensed volume is proportional to the microwave interrogating hot-spot, the nonlinear measurements mainly come from the presence of individual or few dead/live bacteria.

The microfluidic system consisted of a microfluidic circuit and microfluidic channel bonded to the surface of the electrodes. The microfluidic circuit was formed using a pump with pressure/vacuum and flow control (Precigenome, USA), PTFE connectors, and $1/16''$ tubes. These were connected to the inlet and outlet of the microfluidic channel on the electrodes. The microfluidic channel was manufactured using PDMS and standard soft lithography techniques. As illustrated in Fig. 6(b), a channel mold was created in the SU-8 using soft lithography. PDMS was poured onto the mold, and the channel was removed from the mold and glued onto the electrodes using oxygen plasma treatment.

Sample preparation materials and equipment included Escherichia coli (E. coli) strain K-12, Luria-Bertani (LB) broth, and a benchtop shaking incubator (Corning, USA) for bacterial culture. A mixture of ethanol and dimethyl sulfoxide (DMSO) was probed to have nonlinear properties [34]. The measurements were performed in a controlled environment to ensure accuracy and reliability of the results.

A. SAMPLE PREPARATION

In this study, four samples were prepared to deploy nonlinear microwave susceptibility: (i) pure ethanol, (ii) a mixture of Ethanol and DMSO, (iii) live, and (iv) dead E. coli. For the ethanol–DMSO mixture, three sets with different ethanol mole fractions of 1.22, 0.41 and 0.24 were considered.

Live E. coli were cultured in Luria-Bertani (LB) broth at a temperature of 37°C for 24 h. The bacteria were harvested by centrifugation and resuspended in phosphate-buffered saline (PBS). The final concentration of resuspended bacteria was approximately 10^8 cells/mL.

Dead E. coli bacteria were prepared by mixing a 10 mL portion of the live bacterial sample with 40 mL of water. A 1 mL sample was then taken from this mixture and subjected to heat treatment at 80°C for 20 min. Finally, a 100 μL sample of each prepared sample was placed in the sensing region of the electrodes for further analysis.

V. MICROWAVE NONLINEAR EXPERIMENTAL RESULTS

Measurements were conducted using broadband electrodes [33] to assess the third-order intermodulation product power at 5.9 GHz. The results showed that without a sample, the measured power was −98.46 dBm. When Ethanol was introduced as the sample, the power decreased to −112.34 dBm, indicating the loss of ethanol. Subsequently, the introduction of live E. coli as a sample resulted in a power measurement of −90.16 dBm, suggesting that E. coli introduced nonlinearities to the system. Finally, a sample containing a mixture of ethanol and live E. coli was prepared, and the measured power decreased to −105.34 dBm, as shown in Fig. 7.

These findings suggest that the presence of live E. coli introduces nonlinearity to the system, as evidenced by the increase in the measured power compared with the empty electrodes. The decrease in power when ethanol was added to the E. coli sample further supported this observation because

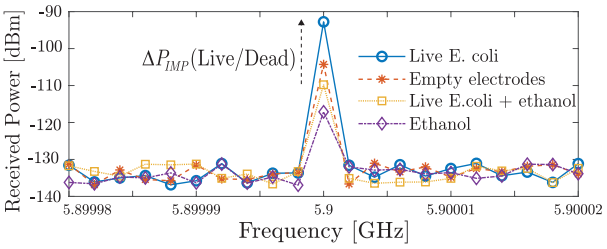

FIGURE 7. Comparison of the microwave nonlinear measurements for the four experiments deployed.

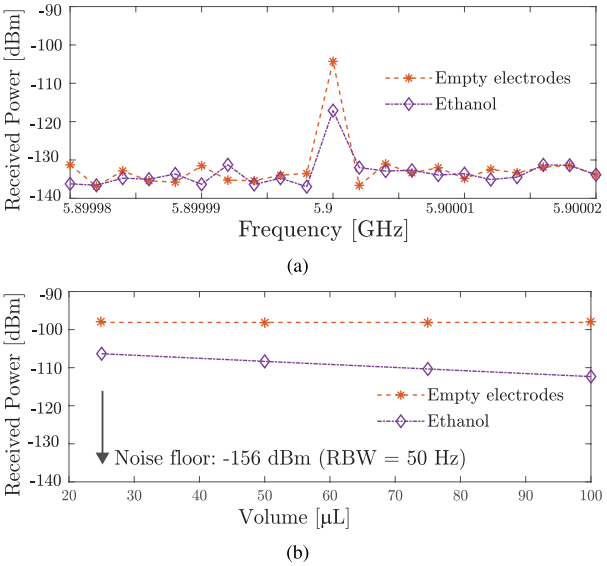

FIGURE 8. (a) Third-order intermodulation products for a empty channel and a 50 µL Ethanol sample. (b) Volume variation of the Ethanol sample (blue line) and reference line of the empty electrodes received power.

of the reduced quantity of living bacteria. Further analysis and discussion of the results are presented in the next section.

To ensure the repeatability of our findings, the experiments were conducted twice over three different days under controlled conditions, meticulously documenting procedures, and controlling variables such as room temperature, humidity, and sample preparation techniques.

VI. DISCUSSION OF RESULTS

A. ETHANOL SAMPLE MEASUREMENT

In the absence of a sample on the electrodes, the peak power of the system was measured as −98.46 dBm. Subsequently, the resolution bandwidth (RBW), measurement span, and value of the internal oscillator attenuator were adjusted to optimize the dynamic range of the measurements. Specifically, the central frequency was set to 5.9 GHz, span was set to 100 kHz, RBW was set to 50 Hz, and attenuator power was adjusted to approximately 20 dB until the optimum mixer level was reached.

Following these adjustments, an expected linear sample, such as ethanol, was placed within the sensing area of the electrodes to perform testing measurements. The peak power measured for the ethanol sample was found to be −112.34 dBm, as shown in Fig. 8(a). Compared to the power

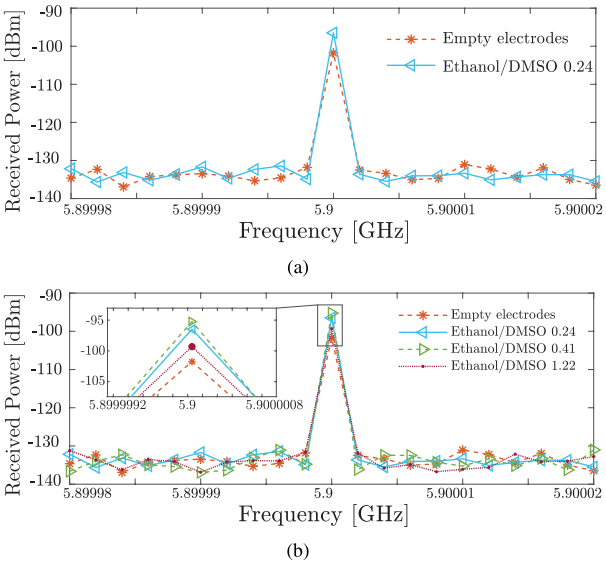

FIGURE 9. (a) Ethanol+DMSO nonlinear response measurment. (b) Intermodulation products for solutions with different Ethanol/DMSO mixtures at Ethanol mole fractions of 1.22, 0.41, 0.24.

measured in the absence of a sample, there was a noticeable reduction in power when the ethanol sample was present. This decrease in power is attributed to the system losses introduced by the ethanol sample. Despite these losses, the output power response maintained a linear trend, underscoring the consistent performance of the system across the varying sample volumes. As the volume of the ethanol sample varied, a corresponding variation in the measured peak power was observed, as shown in Fig. 8(b). This response exhibits linear behavior, indicating a direct proportionality between the sample volume and the measured peak power.

B. ETHANOL-DMSO MIXTURE

To quantify the nonlinearities, a mixture of Ethanol and DMSO with an ethanol mole fraction of 0.24 was utilized as a reference sample. The power requirement associated with this mixture was measured as −95.76 dBm. This process is illustrated in Fig. 9(a), which represents an increase of 3 dB compared to the power measured in the absence of any sample on the electrodes.

This increase in the power signifies the introduction of nonlinear characteristics into the system, which are induced by the presence of a nonlinear sample. To further investigate the effect of nonlinearity, measurements were conducted using ethanol mole fractions of 0.24, 0.41 and 1.22. In this regard, Fig. 9(b) shows the measured output power for different mole fractions, which follows the same trend as that presented in [34].

C. COLI NONLINEAR SUSCEPTIBILITY MEASUREMENTS

Initially, live E. coli was measured to ascertain nonlinear susceptibility. A 50 µL sample of live E. coli was introduced into the sensing region of the electrodes using the microfluidic system. The peak power measured for this sample was −90.16 dBm. Compared to the power measurement obtained in the absence of a sample (−98.46 dBm), there is a notable difference of 8 dB. This variation underscores the nonlinear effects exerted by live E. coli samples.

Subsequently, 50 µL of ethanol was added to the live E. coli sample to ensure that the bacteria were no longer viable. Subsequently, the measured peak power was reduced to −105.23 dBm, which was even lower than the peak power measured in the absence of the sample. This observation can be attributed to the reduction in live E. coli and the loss induced by the presence of bacteria altered in ethanol. Fig. 10(a) provides a visual representation of the peak power measured for empty electrodes, live E. coli, and ethanol-treated E. coli samples.

1) LIVE AND HEAT-KILLED E. COLI MEASUREMENTS

In the final phase of the experiment, a heat-death process was employed to isolate and negate the effects of ethanol on E. coli + ethanol samples. Bacterial samples were prepared as described in Section IV-A. Three samples were measured, live E. coli, dead E. coli, and 100-times diluted dead E. coli in water, to assess the nonlinear susceptibility of the bacteria to the system. The peak power measured for live E. coli was −89.72 dBm, whereas it was −96.23 dBm for heat-killed E. coli and −104.56 dBm for diluted heat-killed E. coli.

These three measurements are shown in Fig. 10(b), along with the reference signal of the empty electrodes. Live E. coli exhibited a variation of approximately 6 dB when compared to heat-killed E. coli, which is in agreement with the theoretical estimation in Section II-B. However, when the dead E. coli sample was diluted, the peak intensity decreased by approximately 15 dB. The diluted samples primarily contained water and inactivated E. coli, both of which were mostly inert. These inert components do not contribute to the signal but instead induce losses in the system, leading to a decrease in the peak signal.

The nonlinear effects of live E. coli (−89.72 dBm) were more pronounced than those of ethanol mixtures, as evidenced by a significant 8 dB difference in power compared to the absence of a sample, indicating strong nonlinear susceptibility. In contrast, the measured output power for heat-killed E. coli −96.23 dBm is comparable to those of ethanol mole fractions of 0.24 and 0.41 (−97 dBm and −95 dBm, respectively), suggesting similar nonlinear characteristics to moderate ethanol concentrations. Diluted heat-killed E. coli shows a peak power of −104.56 dBm, lower than any ethanol mixture, indicating less significant nonlinear effects. Moreover, the latter is comparable to the highest ethanol concentration (1.22, −100 dBm). These findings illustrate a spectrum of nonlinear values, with live E. coli exhibiting the highest nonlinear susceptibility, heat-killed E. coli showing moderate nonlinearity, and diluted heat-killed E. coli showing the lowest.

The peaks presented in Fig. 10(b) (−90 dBm to −110 dBm), above the noise level (−130 dBm), indicate nonlinear susceptibility detection with a difference of more

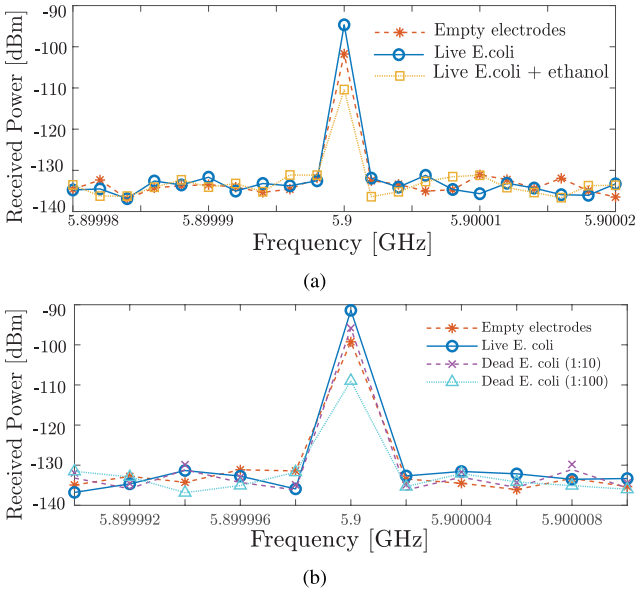

FIGURE 10. (a) PIMP measurement of live E. coli and a mixture of live E. coli and Ethanol. (b) PIMP measured between live E. coli and heat-killed E. coli diluted in water at proportions of 1/10 and 1/100.

than 20 dB. The noise level rises above the standard DANL value of 1 Hz according to equation $10\log_{10}(\text{RBW})$. Hence, increasing the RBW by a factor of 10 increases the noise level by 10 dB.

VII. CONCLUSION

This work demonstrats a method for measuring microwave nonlinear susceptibility in living cells, such as E. coli, based on the principle of intermodulation products. The achieved system sensitivity allows for distinguishing between live and heat-killed bacteria from the nonlinear response resulting from the system. The results obtained have enabled narrowing of the gap between the RF and optical techniques for measuring nonlinear susceptibility. Implementation of the microfluidic system facilitated the precise regulation of the sample volume interfacing with the electrodes. The large bandwidth of the electrodes provides frequency separation between the signals of the two generators, effectively isolating the frequencies and avoiding the individual filtering of each signal.

Therefore, this study has significant implications for the field of cellular biology and related disciplines. In particular, it opens new avenues for studying cellular behavior and responses, potentially leading to advancements in the understanding of cellular processes and mechanisms. These findings raise new questions that merit further research, including the expansion of the range of bacterial species studied to understand how different species respond to microwave-microfluidic systems, improving the sensitivity and resolution of the nonlinearity measurements, or potentially being integrated with other systems such as optical or electrochemical sensors to provide additional information about the bacteria.

REFERENCES

[1] P. M. A. Antony, C. Trefois, A. Stojanovic, A. S. Baumuratov, and K. Kozak, "Light microscopy applications in systems biology: Opportunities and challenges," *Cell Commun. Signaling*, vol. 11, no. 1, p. 24, 2013.

[2] G. Gharib, İ. Bütün, Z. Muganlı, G. Kozalak, İ. Namlı, S. S. Sarraf, V. E. Ahmadi, E. Toyran, A. J. Van Wijnen, and A. Koşar, "Biomedical applications of microfluidic devices: A review," *Biosensors*, vol. 12, no. 11, p. 1023, 2022.

[3] L. Dai, X. Zhao, J. Guo, S. Feng, Y. Fu, Y. Kang, and J. Guo, "Microfluidics-based microwave sensor," *Sens. Actuators A, Phys.*, vol. 309, Jul. 2020, Art. no. 111910.

[4] L. Jasińska and K. Malecha, "Microfluidic modules integrated with microwave components—Overview of applications from the perspective of different manufacturing technologies," *Sensors*, vol. 21, no. 5, p. 1710, Mar. 2021.

[5] C. Palacios, M. Jofre, L. Jofre, J. Romeu, and L. Jofre-Roca, "Superheterodyne microwave system for the detection of bioparticles with coplanar electrodes on a microfluidic platform," *IEEE Trans. Instrum. Meas.*, vol. 71, pp. 1–10, 2022.

[6] M. Jofre, L. Jofre, and L. Jofre-Roca, "On the wireless microwave sensing of bacterial membrane potential in microfluidic-actuated platforms," *Sensors*, vol. 21, no. 10, p. 3420, May 2021.

[7] C. Palacios, M. Jofre, L. Jofre, J. Romeu, and L. Jofre-Roca, "Coplanar electrode near-field radiation optimization for single-cell detection," in *Proc. 17th Eur. Conf. Antennas Propag. (EuCAP)*, Mar. 2023, pp. 1–5.

[8] W. Jung, J. Li, O. Chaudhuri, and T. Kim, "Nonlinear elastic and inelastic properties of cells," *J. Biomechanical Eng.*, vol. 142, no. 10, Oct. 2020, Art. no. 100806.

[9] Y. Bu, L. Li, C. Yang, R. Li, and J. Wang, "Measuring viscoelastic properties of living cells," *Acta Mechanica Solida Sinica*, vol. 32, no. 5, pp. 599–610, 2019.

[10] Y. Chen, X. Wang, J. Liu, Y. Li, Y. Zhang, X. Wang, W. Li, and Q. Dong, "Non-linear cellular dielectrophoretic behavior characterization using dielectrophoretic tweezers-based force spectroscopy inside a microfluidic device," *Micromachines*, vol. 10, no. 12, p. 849, 2019.

[11] V. Kuznetsov and L. Kuznetsova, "RF nonlinear interactions in living cells-I: Nonequilibrium thermodynamic theory," *J. Biol. Phys.*, vol. 45, no. 4, pp. 387–405, 2019.

[12] A. Bartoli, A. Bazzocchi, S. Peli, L. Zanetti-Polzi, S. Corni, A. Alessandrini, and P. Facci, "Measuring vibrational modes in living human cells," *ACS Nano*, vol. 14, no. 3, pp. 3238–3247, 2020.

[13] G. Antonacci, G. Rusciano, P. Capriglione, G. Pesce, M. Pellegrino, F. Merola, M. A. Ferrara, P. A. Netti, and A. Sasso, "Non-contact mechanical and chemical analysis of single living cells by microspectroscopic techniques," *Nature Commun.*, vol. 11, no. 1, pp. 1–10, 2020.

[14] B. Nemet, V. Nikolenko, and R. Yuste, "Second harmonic imaging of membrane potential of neurons with retinal," *J. Biomed. Opt.*, vol. 9, no. 5, pp. 873–881, 2004.

[15] L. Miller, W. Brewer, J. Williams, E. Fozo, and T. Calhoun, "Second harmonic generation spectroscopy of membrane probe dynamics in gram-positive bacteria," *Biophysical J.*, vol. 117, no. 8, pp. 1419–1428, 2019.

[16] V. Parodi, E. Jacchetti, R. Osellame, G. Cerullo, D. Polli, and M. T. Raimondi, "Nonlinear optical microscopy: From fundamentals to applications in live bioimaging," *Frontiers Bioengineering Biotechnol.*, vol. 8, Oct. 2020, Art. no. 585363.

[17] S. Pallen, Y. Shetty, S. Das, J. M. Vaz, and N. Mazumder, "Advances in nonlinear optical microscopy techniques for in vivo and in vitro neuroimaging," *Biophysical Rev.*, vol. 13, no. 6, pp. 1199–1217, 2021.

[18] J. Adur, H. F. Carvalho, C. L. Cesar, and V. H. Casco, *Nonlinear Microscopy Techniques: Principles and Biomedical Applications*, vol. 1. London, U.K.: InTech, 2016, pp. 131–134.

[19] F. L. Labarthet and Y. R. Shen, "Nonlinear optical microscopy," in *Optical Imaging and Microscopy: Techniques and Advanced Systems*. USA: Springer, 2003, pp. 169–196.

[20] B. R. Masters and P. So, *Handbook of Biomedical Nonlinear Optical Microscopy*. London, U.K.: Oxford Univ. Press, 2008.

[21] Z. Cai, L. Liu, F. de Paulis, and Y. Qi, "Passive intermodulation measurement: Challenges and solutions," *Engineering*, vol. 14, pp. 181–191, Jul. 2022.

[22] P. L. Lui, "Passive intermodulation interference in communication systems," *Electron. Commun. Eng. J.*, vol. 2, no. 3, pp. 109–118, Jun. 1990.
[23] Q. Balzano and A. Sheppard, "RF nonlinear interactions in living cells-I: nonequilibrium thermodynamic theory," *Bioelectromagnetics*, vol. 24, no. 7, pp. 473–482, 2003.
[24] Q. Balzano, "RF nonlinear interactions in living cells–II: Detection methods for spectral signatures," *Bioelectromagnetics*, vol. 24, no. 7, pp. 483–488, 2003.
[25] G. Franceschetti and I. Pinto, "Cell membrane nonlinear response to an applied electromagnetic field," *IEEE Trans. Microw. Theory Techn.*, vol. MTT-32, no. 7, pp. 653–658, Jul. 1984.
[26] C. Chen, X. Bai, Y. Ding, and I.-S. Lee, "Electrical stimulation as a novel tool for regulating cell behavior in tissue engineering," *Biomaterials Res.*, vol. 23, pp. 1–12, Dec. 2019.
[27] C. Monzel, C. Vicario, J. Piehler, M. Coppey, and M. Dahan, "Magnetic control of cellular processes using biofunctional nanoparticles," *Chem. Sci.*, vol. 8, no. 11, pp. 7330–7338, 2017.
[28] T. Ma, Q. Ding, C. Liu, and H. Wu, "Electromagnetic fields regulate calcium-mediated cell fate of stem cells: Osteogenesis, chondrogenesis and apoptosis," *Stem Cell Res. Therapy*, vol. 14, no. 1, p. 133, 2023.
[29] N. Nasir and M. A. Ahmad, "Cells electrical characterization: Dielectric properties, mixture, and modeling theories," *J. Eng.*, vol. 2020, pp. 1–17, Jan. 2020.
[30] A. A. Abduljabar, X. Yang, D. A. Barrow, and A. Porch, "Modelling and measurements of the microwave dielectric properties of microspheres," *IEEE Trans. Microw. Theory Techn.*, vol. 63, no. 12, pp. 4492–4500, Dec. 2015.
[31] C. Rinaldi and H. Brenner, "Body versus surface forces in continuum mechanics: Is the Maxwell stress tensor a physically objective cauchy stress?" *Phys. Rev. E, Stat. Phys., Plasmas, Fluids, Rel. Interdiscipl. Topics*, vol. 65, no. 3, 2002, Art. no. 036615.
[32] C. Brosseau and E. Sabri, "Resistor–capacitor modeling of the cell membrane: A multiphysics analysis," *J. Appl. Phys.*, vol. 129, no. 1, 2021, Art. no. 011101.
[33] C. Palacios Arias, M. Jofre, L. Jofre, J. Romeu, and L. Jofre-Roca, "Microwave contactless current-sensing for live/dead differentiation of single bioparticles on a microfluidic platform," *IEEE Trans. Instrum. Meas.*, vol. 72, 2023, Art. no. 8004310.
[34] H. Sun and K. Huang, "Experimental study of dielectric property changes in DMSO–primary alcohol mixtures under low-intensity microwaves," *RSC Adv.*, vol. 5, no. 75, pp. 61031–61034, 2015.

CÉSAR PALACIOS-ARIAS (Student Member, IEEE) received the B.S. degree in electronics and telecommunication engineering from the Private Technical University of Loja, Loja, Ecuador, in 2013, and the M.S. degree in electronics engineering from the University of Calabria, Cosenza, Italy, in 2017. He is currently pursuing the Ph.D. degree with the Department of Signal Theory and Communications, Universitat Politècnica de Catalunya—BarcelonaTech (UPC), Spain. He has held positions at ALCATEL-LUCENT, Corporación Nacional de Telecomunicaciones (CNT), Ecuador. He has collaborated as a Professor with the National University of Chimborazo. Since 2019, he has been a Research and Teaching Staff Member with UPC. His research interests include micro-system design and manufacturing for communication and sensing at microwave, mmwave, optics, and terahertz frequencies.

MARC JOFRE received the M.Sc. degree in electrical engineering (telecom) from Universitat Politècnica de Catalunya—BarcelonaTech (UPC), Barcelona, Spain, jointly with the Technical University of Delft, Delft, The Netherlands, in 2008, and the Ph.D. degree in photonic sciences from the ICFO—The Institute of Photonic Sciences, Castelldefels, Spain, in 2013. Since 2018, he has held different positions at UPC, Fundació Privada Hospital Asil de Granollers (FPHAG), and Max-Planck Institute for Quantum Optics. He has published several peer-reviewed articles and granted/transferred patent applications, and participated in several funded projects (national and international; competitive and non-competitive). He has extensive experience in innovation, research, project management, intellectual property, exploitation of quantum technologies for communication and sensing systems, physical characterization of nonlinear materials, biophysical detectors, platforms for the quantification of microorganisms, and health technology.

MARÍA-JOSÉ LÓPEZ (Student Member, IEEE) was born in Ecuador. She received the degree in electronic engineering (telecommunications and networks) from the Higher Polytechnic School of Chimborazo, in 2013, and the master's degree in telecommunications engineering from the University of Calabria, Italy, in 2017. She is currently pursuing the Ph.D. degree with Universitat Politècnica de Catalunya—BarcelonaTech (UPC), Barcelona, Spain. From 2013 to 2019, she taught at the Faculty of Computer Science and Electronics, the Faculty of Sciences, and the Faculty of Livestock Sciences, Polytechnic School of Chimborazo. She is with the AntennaLab Group and the ComSense Lab Group, Department of Signal Theory and Communications (TSC), UPC. She conducted a research stay with the Millimeter-Wave Antennas and Integrated Circuits Laboratory, University of Calabria. In addition, she has completed several complementary training courses in the areas of innovation and vocational training for employment. Since 2021, she has been a part of the M2m Program, UPC, where she is the professional network for women, "Women in Business," and is a volunteer at the Young IT Girl in Spain. Her academic work is focused on the manufacture and use of sensors for physiological measurements in smart cars.

YOUNESS AKAZZIM (Student Member, IEEE) received the License degree in electronics and the M.Sc. degree in telecommunication systems engineering from Abdelmalek Essaâdi University, Morocco, in 2016 and 2018, respectively. He is currently pursuing the Ph.D. degree with the Signal Theory and Communications (TSC) Department, within the research group of CommSensLab, Universitat Politècnica de Catalunya—BarcelonaTech (UPC), Barcelona, Spain. He was a Research Support Technician with the Signal Theory and Communications (TSC) Department, UPC, from 2020 to 2021. In 2017, he joined the Information and Telecommunication Systems Laboratory (LaSIT), Faculty of Sciences, Tetouan, Morocco, where he has been a Research Assistant. He has been awarded the Erasmus + Mobility Grant. He is currently involved in human body parts functionality monitoring using microwave imaging.

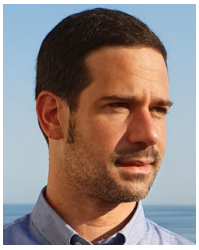

LLUIS JOFRE received the degree in mechanical engineering from Universitat Politècnica de Catalunya—BarcelonaTech (UPC), Barcelona, Spain, jointly with the KTH Royal Institute of Technology, Sweden, in 2008, and the Ph.D. degree in fluid mechanics and thermal engineering from UPC, in 2014. From 2015 to 2020, he was a Postdoctoral Researcher with the Center for Turbulence Research, Stanford University, USA. He is currently a Beatriz Galindo Professor with the Department of Fluid Mechanics, UPC. His main research interests include microfluidics, biophysical fluids, high-pressure supercritical flows, two-phase flows, modeling and computational studies of turbulence in multiphysics environments, uncertainty quantification, and data science in fluid mechanics. He has contributed to 40 peer-reviewed papers and more than 50 conferences, and participated in 15 funded competitive/non-competitive projects nationally and internationally.

JORDI ROMEU (Fellow, IEEE) received the Ingeniero de Telecomunicación and the Doctor Ingeniero de Telecomunicación degrees from the Universitat Politècnica de Catalunya (UPC)-BarcelonaTech, Barcelona, Spain, in 1986 and 1991, respectively. In 1985, he joined the AntennaLab, Signal Theory and Communications Department, UPC, where he is currently a Full Professor involved in antenna near-field measurements, antenna diagnostics, and antenna design. In 1999, he was a Visiting Scholar with the Antenna Laboratory, University of California at Los Angeles, Los Angeles, CA, USA, on a NATO Scientific Program Scholarship, and the University of California at Irvine, Irvine, CA, USA, in 2004. He holds several patents. He has published 60 refereed articles in international journals and 80 conference proceedings. He was a Grand Winner of European IT Prize, awarded by European Commission for his contributions to the development of fractal antennas, in 1998.

LUIS JOFRE-ROCA (Life Fellow, IEEE) received the M.Sc. and Ph.D. degrees in electrical engineering (telecommunication engineering) from the Technical University of Catalonia—BarcelonaTech (UPC), Barcelona, Spain, in 1978 and 1982, respectively. Since 1982, he has been a part of the Communications Department, Telecommunication Engineering School, UPC, first as an Associate Professor and since 1989, as a Full Professor. He was a Visiting Professor with Ècole Supèrieure d'Electricitè Paris, Gif-sur-Yvette, France, from 1981 to 1982, where he was involved in microwave antenna design and imaging techniques for medical and industrial applications. From 1986 to 1987, he was a Visiting Fulbright Scholar with Georgia Institute of Technology, Atlanta, GA, USA, where he was involved in antenna near-field measurements and electromagnetic imaging. From 2000 to 2001, he was a Visiting Professor with the Electrical and Computer Engineering Department, University of California at Irvine, Irvine, CA, USA, where he was involved in reconfigurable antennas and microwave sensing in civil engineering structures. Since 2003, he has also been the Director of the UPC-Telefonica Chair on Information Society Future Trends. He was a Principal Investigator of the 2008–2013 Spanish Terahertz Sensing Laboratory Consolidator Project, the Research Leader of the 2017–2020 ComSense Lab Maria de Maeztu Project, the Academic Director of the Consortium for Future Urban Mobility (CARNET), and the Chairperson of the EIT-Urban Mobility European Association. He has authored more than 200 scientific and technical articles, reports, and chapters in specialized volumes. His current research interests include antennas, electromagnetic scattering and imaging, and system miniaturization for wireless sensing in industrial and bio-applications from microwaves to terahertz frequencies.